Special Issue Article

Institution of MECHANICAL ENGINEERS
Journal of MECHANICAL ENGINEERING SCIENCE

Proc IMechE Part C:
J Mechanical Engineering Science
0(0) 1–13

DOI: 10.1177/0954406217723365
journals.sagepub.com/home/pic
SAGE

Some comments on the energy-absorbing effectiveness factor

Norman Jones

Abstract

This paper discusses the energy-absorbing effectiveness factor which provides a ratio between the energy absorbed in a structural system with the total potentially available elastic and plastic strain energies in all the materials used in the construction. Experimental and numerical predictions for the factor are expressed in terms of the solidity ratio, or relative density, for various tubes and multicellular sections subjected to static and impact axial loadings. The factor illustrates the effectiveness of multicellular systems when compared to simple regular geometries. The effect of infilling is discussed along with several other factors. The energy-absorbing effectiveness factor is a useful dimensionless quantity to assist in the choice of efficient designs of structural systems which require an energy-absorbing capability.

Keywords

Energy-absorbing effectiveness factor, square, circular, triangular, polygonal, multicellular tubes, tube infilling, impact loading, static loading

Date received: 11 February 2017; accepted: 7 July 2017

Introduction

The amount of energy which can be absorbed in structural systems and energy-absorbing devices are important for studies in the structural crashworthiness field and safety calculations in many areas. It is useful to have a criterion for assessing the effectiveness of an energy-absorbing system which motivated the following definition for an energy-absorbing effectiveness factor[1]

$$\psi = \frac{\begin{array}{c}\textit{total elastic and plastic strain energies}\\ \textit{absorbed by a structural system}\end{array}}{\begin{array}{c}\textit{potential energy absorption in the total volume}\\ \textit{of material in a system up to failure in tension}\end{array}} \quad (1)$$

This factor could be calculated for structures made from any material such as composite materials, which have been used extensively throughout engineering including many structural crashworthiness protection studies,[2] etc. The energy absorbed in the material up to failure in the denominator of equation (1) could be found for a variety of failure modes, but the failure in tension is used in this paper because it is focussed on ductile materials and most experimental studies in this area only report the results from standard uniaxial tensile tests.

It is the purpose of this dimensionless number to reveal the efficiency of an energy-absorbing system by comparing the proportion of the ductile strain energy extracted from the total energy potential of all the material used in its construction. Therefore, the denominator includes the energy potential of all components, such as any internal fillings and the energy potential of all the different materials that might be used in the construction. Thus, systems having different geometries and made of different materials (including combinations of several materials) can be compared and the design having the largest value of ψ is the most effective and also the most environmentally acceptable in the sense of utilising the minimum material resources for a specified energy absorbing application. In practical design, this factor could be considered along with all other well-known parameters such as cost, etc. Equation (1) may be used for both static and dynamic loadings.

The energy-absorbing effectiveness factor ψ was used in Hsu and Jones[3] to examine the static and

Impact Research Centre, Department of Engineering, University of Liverpool, Liverpool, UK

Corresponding author:
Norman Jones, Department of Engineering, University of Liverpool, Harrison-Hughes Building, Liverpool L69 3GH, UK.
Email: njonesijie@gmail.com

dynamic (up to 13.3 m/s) axial crushing behaviour of stainless steel, mild steel and aluminium alloy thin-walled circular tubes. It transpired for both loadings that the aluminium alloy tubes have a significantly higher value of ψ than the stainless steel and mild steel tubes. The ψ values for the stainless steel tubes are the smallest, while the values of ψ for the mild steel tubes lie between those for the other two materials. On the other hand, the energy absorbed per unit volume is lowest for the statically crushed aluminium alloy tubes and highest for the stainless steel tubes, though the energy absorbed per unit mass of the aluminium alloy tubes is only slightly greater than the corresponding value for the stainless steel tubes. This situation occurs because the stainless steel and the mild steel tubes have higher plastic strain energies to failure than is required for a ductile crushing response of the tubes. In other words, energy-absorbing systems made of stainless steel and mild steel for this particular problem use the material less effectively than those made from the aluminium alloy.

Further comments and observations on the energy-absorbing effectiveness factor were presented in Jones[4] wherein several other geometries were examined including square tubes, top-hat, double-hat and hexagonal sections. It was observed for mild steel that ψ is larger for the thin-walled square tubes than for the top-hat and double-hat sections and all have smaller values of ψ than for the thin-walled circular tubes when subjected to static or impact axial crushing loadings. The additional material in the flanges of the top-hat and double-hat sections does not provide a sufficient increase in the energy absorbed to lead to increased values of ψ when compared with a simple thin-walled square section.

Jones[1] explored the trend of the energy-absorbing effectiveness factor, ψ, for several thin-walled geometries with respect to the plastic flow stress, axial impact velocity and tube geometry (thickness H, radius R for circular tubes, side length C and thickness H for square tubes). The influence of longitudinal stiffeners on the values of ψ for thin-walled circular and square tubes was studied, as well as the enhancement of ψ due to aluminium alloy foam fillings in circular and square tubes. Chen and Wierzbicki[5] presented a theoretical analysis which is based on a rigid, perfectly plastic material for square tubes having two or three internal cells. The associated values of ψ are reported in Jones[1] together with the corresponding values when the cells are filled with an aluminium foam material. This gives rise to a significant enhancement of ψ as revealed in table 2 of Jones[1] and as discussed in '*Multicellular sections*' section.

Within recent years many experimental, theoretical and numerical studies have been reported on the static and dynamic crushing behaviour of energy-absorbing systems having various designs and made from a variety of materials (e.g. Belingardi et al.[6]). The behaviour of these systems has been explored with the aid of various well-known design parameters as in Xiang et al.,[7] for example. It is the object of this article to examine some recent studies on axially crushed tubes having various cross-sectional shapes from the perspective of the energy-absorbing effectiveness factor, ψ, which is defined by equation (1).

Energy-absorbing effectiveness factor

Equation (1) for an energy-absorbing system can be written in the form

$$\psi = \frac{\int_o^{\delta_f} P d\delta}{\sum_{i=1}^{n} V_i \int_o^{\varepsilon_{ri}} \sigma d\varepsilon}, \tag{2}$$

where P is the axial crushing force and δ is the corresponding axial crushing displacement which has a final value δ_f. The integral in the denominator of equation (2) is the potentially available energy which could be absorbed in the total volume of material in all parts of a structural system, $\sum_{i=1}^{n} V_i$, up to rupture in standard uniaxial tensile tests on specimens which are made from the same n different materials in an energy-absorbing system. Equation (1) is also valid for energy-absorbing structural systems subjected to dynamic loads and a dynamic energy-absorbing effectiveness factor, ψ', is defined, in Hsu and Jones.[3]

Several simpler forms of equation (2) are developed, in Jones,[4] for the static and impact axial loading of energy-absorbing systems made from thin-walled sections.

In most published experimental studies, only the static yield (σ_y) and ultimate tensile (σ_u) stresses are reported for the materials, sometimes together with the uniaxial tensile engineering rupture strain (ε_r). The stress values can be used to estimate the mean static and dynamic flow stresses σ_o and σ'_o when disregarding material strain rate effects. Thus, for an energy-absorbing system made from a single material, it might be assumed that

$$\psi = \frac{P_m \delta_f}{\sigma_o A L \varepsilon_r} \tag{3}$$

and

$$\psi' = \frac{GV_o^2/2 + Gg\delta_f}{\sigma'_o A L \varepsilon_r} \tag{4}$$

for the static and impact cases, respectively, where A is the cross-sectional area and L is the initial axial length of an energy absorber.

If the effective crushing distance ratio is taken as $\delta_e/L \approx 3/4$[4] and $\delta_f = \delta_e$, then the length L of an energy absorber in equations (3) and (4) can be replaced by $4\delta_f/3$ giving

$$\psi = \frac{3P_m}{4A\sigma_o\varepsilon_r} \tag{5}$$

and

$$\psi' = \frac{3GV_o^2}{8\sigma_o A\delta_f \varepsilon_r} \tag{6}$$

if any material strain rate sensitivity effects are neglected, that is σ_o' is taken as the mean static flow stress σ_o, and the additional potential energy of the mass due to the axial crushing of the energy absorber is neglected when compared with the initial kinetic energy. The mean flow stress in equations (3) and (6) could be taken as $(\sigma_y + \sigma_u)/2$ to approximate the influence of material strain hardening effects in the corresponding integral in the denominator of equation (2).

The solidity ratio, or relative density,[8,9] has been used extensively in the structural crashworthiness field and is defined as

$$\phi = \mathrm{A}/\mathrm{A_e} \tag{7}$$

where A is the cross-sectional area of a thin-walled section and $\mathrm{A_e}$ is the area enclosed by the cross-section. Thus

$$\phi = 2\pi\mathrm{RH}/\pi\mathrm{R}^2, \quad \text{or} \quad \phi = 2\mathrm{H}/\mathrm{R} \tag{8}$$

for thin-walled circular tubes of radius R and wall thickness H. Similarly, for a thin-walled square tube

$$\phi = 4\mathrm{H}/\mathrm{C} \tag{9}$$

where C is the length of a side. Clearly, equation (7) can be used to obtain ϕ for any cross-sectional shape.

It is unusual for complete information to be available on the material properties which allow an accurate value of the denominator of equation (2) to be calculated, particularly for dynamic loadings. Thus, approximations are introduced such as a mean flow stress taken as the average of the yield and ultimate stresses, as mentioned earlier. It is then possible that an approximation in the denominator of equation (2) could lead to a value of the energy absorbing effectiveness factor which is larger than unity, as observed in some later calculations. This aspect is discussed further in '*Discussion*' section.

Square tubes

It was reported previously in Jones[4] that the mild steel square box sections crushed axially with static loads have $\psi = 0.98$,[10] $\psi = 0.765$ (average)[11] and $\psi = 0.29$[12] for C/H = 22, 31.3 (average) and 48.4, or $\phi = 0.182$, 0.128 and 0.083, respectively. In the associated impact cases, $\psi = 1.28$, $\psi = 1.08$ and $\psi = 0.53$ for the increasing values of C/H, or decreasing values of ϕ given above.

Di Paolo and Tom[13] reported on the quasi-static axial crushing characteristics of square tubes made from two plain low-carbon steels (ASTM A36 and ASTM A513) and two austenitic stainless steels (AISI 316 and AISI 304). The energy-absorbing effectiveness factor ψ can be estimated from the experimental data. It turns out that $\psi = 0.53$ and $\psi = 1.21$ for the low-carbon steels ASTM A36 and ASTM A513, respectively. The significantly different values for ψ occur principally because the rupture strain for the ASTM A513 steel is about one-half the corresponding value for ASTM A36. In other words, the ASTM A36 square tube has a greater energy-absorbing capacity than is required to absorb the axial crushing energy due to the axial force acting on the tube and therefore has more material than is necessary. Both stainless steels have smaller energy-absorbing effectiveness factors, namely $\psi = 0.44$ (stainless steel 316) and $\psi = 0.36$ (stainless steel 304), mainly because of the larger rupture strains and larger flow stresses. These results indicate that the two low-carbon steels are more effective than the two studied stainless steels. Incidentally, the solidity ratios of the square tubes are between 0.11 and 0.12.

The values of ψ and ϕ are calculated for some experimental results on the static and impact loadings of square tubes and are plotted in Figure 1(a) for mild steel,[4] Q235 steel,[14] St37 steel[15] and high strength steel.[4] The solidity ratio $\phi = 4\mathrm{H}/\mathrm{C}$ is used for the

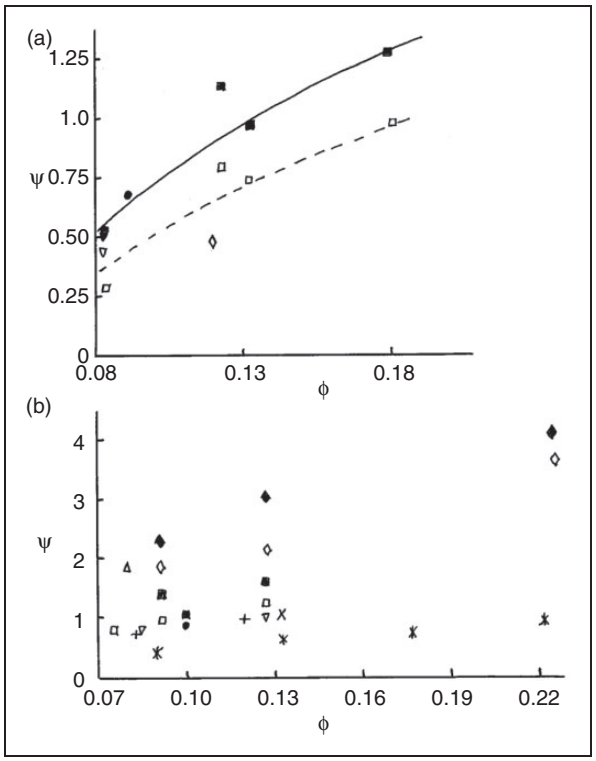

Figure 1. Energy-absorbing effectiveness factor, ψ, for square tubes. (a) Steel. Static loadings – □: mild steel table 2 of Jones,[4] ∇: high strength steel table 2 of Jones,[4] ◇: Q235 steel.[14] Impact loadings – ■, ▼ correspond to □, ∇, respectively: • St37.[15] (b) Aluminium alloy. Static loadings – □, ◇,[4] x,[16] ✱,[17] +,[18] △,[19] ∇.[20] Impact loadings – ■, ◆,[4] •.[21]

abscissa. Despite the different steel specifications, it is evident that the experimental results follow reasonable curves through both the static data and the impact data. It is observed that the energy-absorbing effectiveness factor decreases as C/H increases or ϕ decreases, for both static and impact loadings.

Previous studies have been conducted on the static crushing behaviour of aluminium alloy 6060T4 square tubes.[22] It can be shown from these results that $\psi = 0.97$ for C/H = 43.3 ($\phi = 0.092$) and $\psi = 1.24$ for C/H = 31.6 ($\phi = 0.127$). Square tubes made from aluminium alloy 6060T6 were studied in literature[22,23] and calculations predict that $\psi = 1.84$, 2.17 and 3.64 for C/H = 43.2, 31.5 and 17.8, or $\phi = 0.093$, 0.127 and 0.225, respectively. These values again reveal a trend of decreasing ψ with an increase in C/H, or decrease in ϕ, as observed for the steel boxes in Figure 1(a), but the values are larger principally because of the smaller fracture strains for the aluminium alloys leading to a more effective use of the material.

Figure 1(b) contains a collection of experimental data for aluminium alloy square tubes, but the results show greater scatter than in Figure 1(a) for steel, probably because the test specimens are made from seven different aluminium alloys. Nevertheless, it is evident that the values of ψ for the low-velocity impact loadings do lie above the corresponding static values for similar values of ϕ.

Zhang et al.[16] have explored the static axial crushing behaviour of square tubes with wall thicknesses that vary linearly across the tube width. They are made from aluminium alloy 6061O. One set (simple surface gradient, SSG) is square on the outside and octagonal on the inside, while the other set (double surface gradient, DSG) is octagonal on both the inside and outside surfaces. In both cases, the thinnest wall thicknesses are at the centres of the sides (0.6–1.0 mm), while they are thickest at the corners (1.4–1.8 mm). Regular uniform thickness (1.2 mm) square tubes are tested for comparison purposes and all tubes have the same average thickness of 1.2 mm giving a solidity ratio $\phi = 0.133$. It can be shown that the tests on two regular square tubes give rise to $\psi = 1.04$ and $\psi = 1.15$, or an average of $\psi = 1.10$, approximately. All of the SSG and DSG tubes have higher values of ψ and lie within the range $1.23 \leqslant \psi \leqslant 1.47$, where the largest value is associated with a DSG tube having the thickest corners (1.8 mm) and the thinnest section (0.6 mm) at the centre of the sides. Thus, by simply redistributing the material in a tube it can be made about 34% more effective for the same amount of material.

Zhang and Zhang[17] have reported some experimental static axial crushing data on aluminium alloy 6061O square tubes having various thickness configurations. The thicknesses on opposite sides of a square cross-section (t_1) are equal, while those on the adjacent opposite sides (t_2) are also equal but different from t_1, except for uniform square tubes with $t_1 = t_2$. It transpires that ψ generally increases with increase in $t_1 + t_2$ from $\psi = 0.39$ for $t_1 = t_2 = 0.8$ mm to $\psi = 1.35$ for $t_1 = t_2 = 2.4$ mm and all the other cases lie between these two extremes. The other uniform cases give $\psi = 0.60$, 0.76 and 0.91 for $t_1 = t_2 = 1.2$, 1.60 and 2.0 mm, respectively. Thus, it appears that ψ is directly proportional to the cross-sectional area of the square tubes regardless of the relative values of t_1 and t_2. In other words, it is more effective to thicken tubes in the sense that the additional material is more than compensated by an increase in the energy absorbed. These results reveal that ψ increases with the solidity ratio ϕ (0.089–0.267), though it is evident from Figure 1(b) that they are smaller than all of the other results.

It can be shown from equation (9.41) in Jones[8] that the mean crushing force P_m for a square tube varies as $H^{5/3}$ when all the other parameters remain constant. Thus, equation (5) gives ψ varying as $H^{2/3}$, while ϕ is proportional to H according to equation (9). This theoretical analysis predicts that the thicker tubes have larger values of ψ and ϕ than thinner tubes when the other parameters remain unchanged. For example if H is doubled, then ψ increases by a factor 1.587 and ϕ is doubled.

Circular tubes

Yamashita et al.[18] have reported some experimental test results on the static axial crushing behaviour of circular and square thin-walled tubes made from aluminium alloy 6063. Using the data presented in this paper and taking an effective crushing distance equal to 0.75L gives $\psi = 1.30$, 1.71, 1.94 and 2.17 for circular tubes having $\phi = 0.04$, 0.06, 0.09 and 0.12, respectively. Similarly, $\psi = 0.73$ and $\psi = 0.93$ for the square tubes with $\phi = 0.083$ and 0.124, respectively. A single experiment on a circular tube subjected to an impact loading at 10 m/s has an estimated value of $\psi = 2.46$ for $\phi = 0.12$.

The machining of grooves into the walls of steel cylindrical tubes has been studied by Salehghaffari et al.[24] to see if the energy absorbing characteristics under quasi-static axial compressive loading can be enhanced. It turns out that ψ increases from 0.26 to 0.54 for the test specimens having 5 or 6 grooves and labelled S1 to S6, respectively. The associated values of ϕ are 0.06 to 0.08, approximately. These values contrast with $\psi = 1.02$ and $\psi = 0.78$ for the steel cylindrical tube specimens without grooves and having $\phi = 0.07$ and $\phi = 0.11$, respectively. Thus, the values of ψ reveal clearly that this particular design, according to this criterion, is not an efficient design. This situation occurs because the additional material between the grooves does not contribute to the absorption of crushing energy.

Zhang and Yu[25] have conducted static axial crushing tests on thin-walled cylindrical tubes made from tin (mild steel) beverage cans. The tubes were

pressurized with air up to 9 bar and the energy-absorbing effectiveness factors ψ can be calculated from their data and are presented in Figure 2. It is evident from this figure that ψ increases with the internal pressure p and that the two cases with $\phi = 0.0159$ and 0.0134 are similar, while the results associated with $\phi = 0.0114$ are higher. This difference is related to the fact that the rupture strain $\varepsilon_r = 0.13$ according to the tensile test curves in figure 3 of Zhang and Yu[25] for the material associated with $\phi = 0.0114$ is significantly smaller than those associated with the other two cases ($\varepsilon_r = 0.185$, 0.195). It should be noted that the energy required to pressurize the tubes should be added to the denominator of equation (2) which would lead to smaller values of the energy-absorbing effectiveness factor, ψ, than those given in Figure 2.

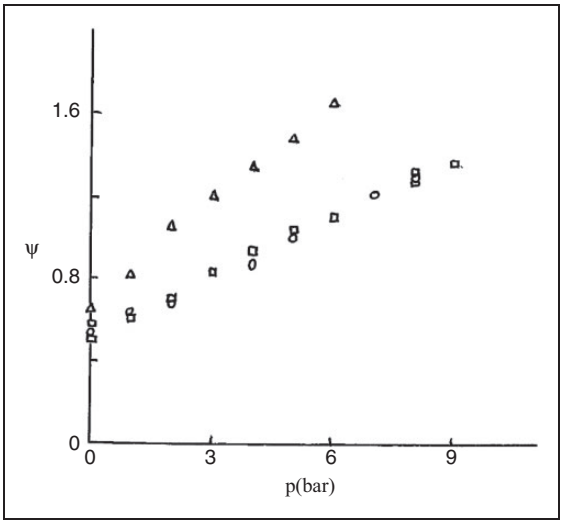

Figure 2. Energy-absorbing effectiveness factor versus internal pressure in circular tubes.[25] ○, □ and Δ correspond to tubes having $\phi = 0.0159$, $\phi = 0.0134$ and $\phi = 0.0114$, respectively.

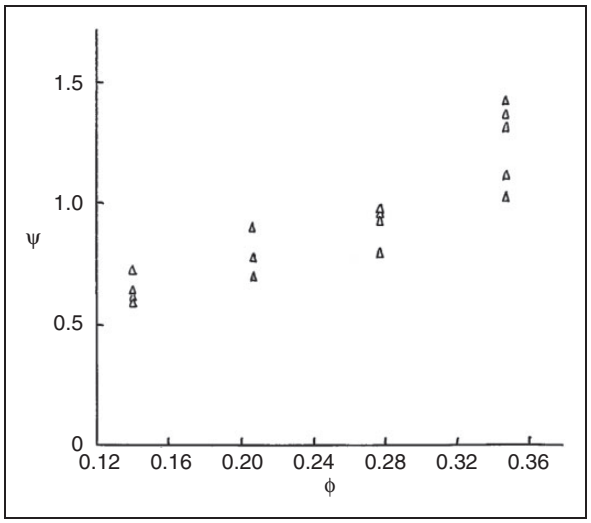

Figure 3. Experimental values of the energy-absorbing effectiveness factor versus the solidity ratio for triangular tubes made from Q235 steel and crushed axially.[27]

Recently, Hu et al.[26] have studied the problem considered in Zhang and Yu[25] by extending their theoretical analysis and presenting calculations using the numerical scheme ANSYS LS-DYNA. They discussed the associated symmetric and non-symmetric deformation modes and examined the variations in the capacity of the tube wall for higher internal pressures than those examined in Zhang and Yu.[25]

Triangular tubes

Hong et al.[27] have conducted quasi-static axial compression tests on tubes having triangular-shaped cross-sections and made from Q235 steel. The test specimens underwent progressive crushing and bottomed-out at about 75% of the initial tube length with the actual values being given in table 2 of their paper together with other experimental details. This information may be used to calculate the energy-absorbing effectiveness factor, ψ, as well as the solidity ratio, ϕ, for the cross-sections. It is evident from Figure 3 that ψ increases with an increase in ϕ so that the thickest tubes (2.5 mm) have an effectiveness which is about double the thinnest specimens (1 mm) and therefore make a more efficient use of the material.

Fan et al.[28] have presented a theoretical rigid, perfectly plastic analysis for a thin-walled triangular tube subjected to static axial crushing loads. In addition, a finite-element numerical procedure was used to predict the load-displacement behaviour. Ten experimental tests were conducted by the authors on low carbon steel (ASTM A36) triangular tubes which responded with folds which did not form sequentially, in contradistinction to the theoretical analysis. In fact, the experimental results in figures 11 and 12 of Fan et al.[28] reveal a high initial peak force with a sharp reduction to a much lower force for the remaining axial crushing displacement. This behaviour possibly develops because the initial side lengths of the triangular sections varied between 44% and 66% of the corresponding initial axial length. The authors conducted a numerical calculation using ABAQUS on a longer triangular tube having an initial length about three times the side length, and these results did show the sequential folding predicted by the theoretical method. Moreover, the theoretical rigid-plastic procedure provides reasonable predictions for the mean crushing force observed in the numerical calculations. However, no experimental results were reported for the longer triangular tubes.

Multicellular sections

Zhang and Zhang[29] have conducted static axial crushing tests on aluminium alloy 6061O columns having

various cellular cross-sections. They observed that multicellular columns are much more efficient energy absorbers than single cellular columns under static axial compression. The energy-absorbing effectiveness factors can be calculated from the data. They ranged from $\psi = 1.03$ for square ($C/H = 30$, $\phi = 0.133$) and $\psi = 1.15$ for hexagonal ($\phi = 0.077$) single cellular sections, to $\psi = 3.21$ for a square section with square boxes in each corner ($\phi = 0.222$). It is interesting to observe that two of the sections with $\phi = 0.20$ were constructed from the same amount of material as used in the hexagonal section, but they had significantly higher energy-absorbing effectiveness factors of $\psi = 1.83$ and $\psi = 2.17$.

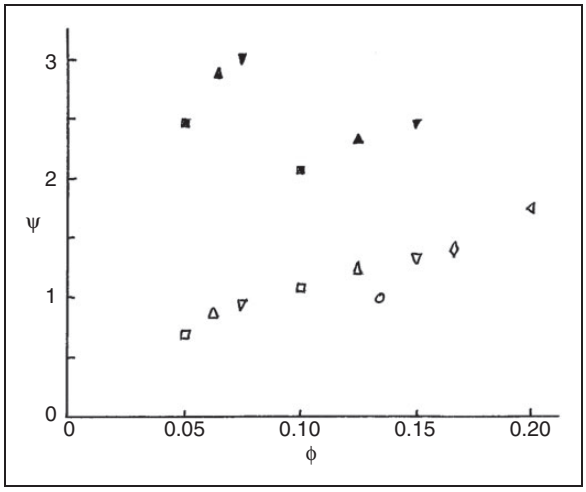

Figure 4. Energy-absorbing effectiveness factor versus solidity ratio. The numerical predictions[5] for single-cell (□), double-cell (△) and triple-cell (▽) cross-sections of AA6061T4 square tubes crushed axially. Filled symbols are for corresponding tubes filled with aluminium foam.[5] ○, ◇ and ◁ are experimental values[29] for single-cell, double-cell and triple-cell square tubes made from AA6061O.

Thus, the energy-absorbing effectiveness factor clearly reveals the superiority of multicellular sections over single cellular sections and shows the importance of the disposition of the internal structure. Nevertheless, this advantage is less clear in Figure 4 where the theoretical predictions of Chen and Wierzbicki[5] (see table 2 of Jones[1] for calculation of ψ) and the experimental values of Zhang and Zhang[29] are plotted for the static axial crushing of square tubes and of square tubes with double and triple cells which are illustrated in Figure 5. It is evident that the theoretical calculations of Chen and Wierzbicki[5] for aluminium alloy 6061T4 follow closely the experimental results presented in Zhang and Zhang[29] on aluminium alloy 6061O tubes and that the advantage of multicellular square tubes is related to the larger values of solidity ratio when compared to the values for the corresponding regular square tube results. However, it is noted from equations (2), (3) and (5) that the mean crushing forces increase with ψ so that it might be necessary in some cases to limit the associated decelerations when multicellular systems are used for safety purposes in passenger transportation systems. A reduction in the magnitude of the deceleration could be achieved with the same structural multicellular design, but with thinner sections.

As noted previously, equation (1) is valid for a wide range of energy-absorbing systems including thin-walled sections which are filled with a foam material, for example. The potential energy-absorbing capacity of any infilling material would be added to the denominator of equations (1) and (2).

Chen and Wierzbicki[5,30] have explored the effect of infilling the sections with lightweight cellular materials, such as an aluminium foam, as discussed in Jones.[1] Figure 4 reveals, from the viewpoint of the static energy-absorbing effectiveness factor, that it is advantageous to have three cells rather than two and it is a further advantage to have a foam-filling.

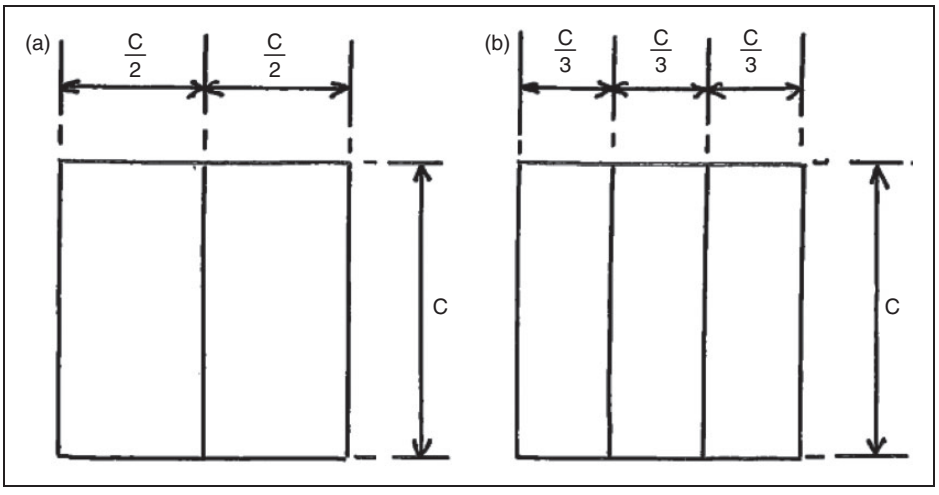

Figure 5. Cross-sections of (a) double-cell and (b) triple-cell square tubes.

It is interesting to observe from Figure 4 for a given geometry that ψ decreases for infilled sections as the solidity ratio ϕ increases. This trend is opposite to that shown in Figure 4 for empty sections that have an increase in ψ with an increase in ϕ. It is possibly due to the interaction effect between the foam-filling and the tube wall being less significant for thicker and therefore stronger tubes relative to the foam strength (i.e. larger values of ϕ).

Zhang et al.[31] used a superfolding theory to study the behaviour of aluminium alloy 6060T4 multicellular square columns under dynamic axial crushing forces. It is estimated that the energy-absorbing effectiveness factor $\psi = 0.90$ for a square tube, while $\psi = 1.32$, 1.66, 1.74 and 1.81 for square tubes with 2×2, 3×3, 4×4 and 5×5 cells, respectively. All cases have the same solidity factor $\phi = 0.075$. The numerical scheme shows that the geometries are stable and that adding internal web arrangements is effective. The 2×2 and 3×3 multicellular cases are illustrated in Figure 6. It is observed from the numerical results, which are plotted in Figure 7, that ψ for the aluminium alloy 6060T4 sections with $\phi = 0.075$ and subjected to impact loadings (10 m/s) are tending towards a saturation value for the more complex sections. It is also noted in Figure 4 (AA6061T4, AA6061O) that the experimental and numerical values for ψ increase with ϕ for the static loading of double and triple cell cross-sections.

The experimental value $\psi = 2.17$ was obtained from Zhang and Zhang's experimental results[29] for a 2×2 section made from aluminium alloy 6061O and having $\phi = 0.20$ and when loaded statically. It is evident from Figure 4 that the value of ψ at $\phi = 0.20$ is about 0.75 higher than the value for ψ at $\phi = 0.075$ for a triple-cell square tube. Thus, the experimental result from Zhang and Zhang[29] is reasonably consistent with the theoretical result in Figure 7 for the 2×2 section (i.e. $\psi = 2.17 - 0.75 = 1.42$ which is to be compared with $\psi = 1.32$).

The experimental tests by Alavi Nia and Parsapour[32] give $\psi = 0.61$ for a 2×2 section loaded statically and had $\phi = 0.012$. Now again the comparison with the results in Figure 4 suggests by extrapolation that ψ might increase by about 0.60 when ϕ increases from 0.012 to 0.075. This suggests that $\psi = 1.21$, approximately, which is slightly lower than $\psi = 1.32$ in Figure 7.

The numerical results by Tang et al.[33] for the impact loading of 2×2 sections made from aluminium alloy 6060T4 predict that $\psi = 1.78$ for $\phi = 0.10$. Again using the results in Figure 4, it is expected this value should be about 0.20 smaller at $\phi = 0.075$ which suggests $\psi = 1.58$ at $\psi = 0.075$. This modified experimental value is to be compared with the theoretical value of $\psi = 1.32$ in Figure 7.

Alavi Nia and Parsapour[34] have reported the results of two experimental tests on aluminium alloy

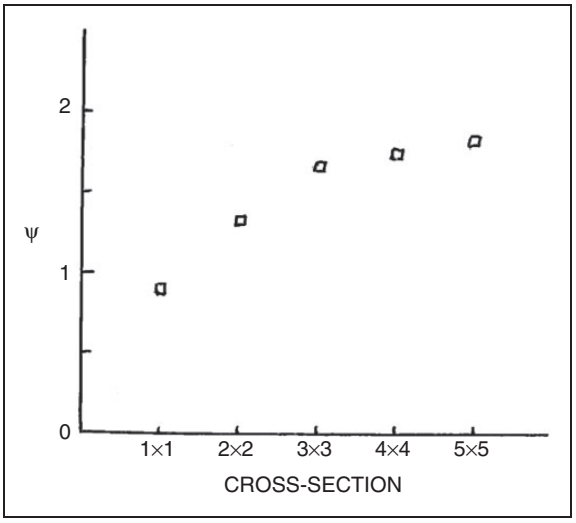

Figure 7. Energy-absorbing effectiveness factor versus cross-sections of multicellular square tubes made from AA6060T4 and having $\phi = 0.075$.[31]

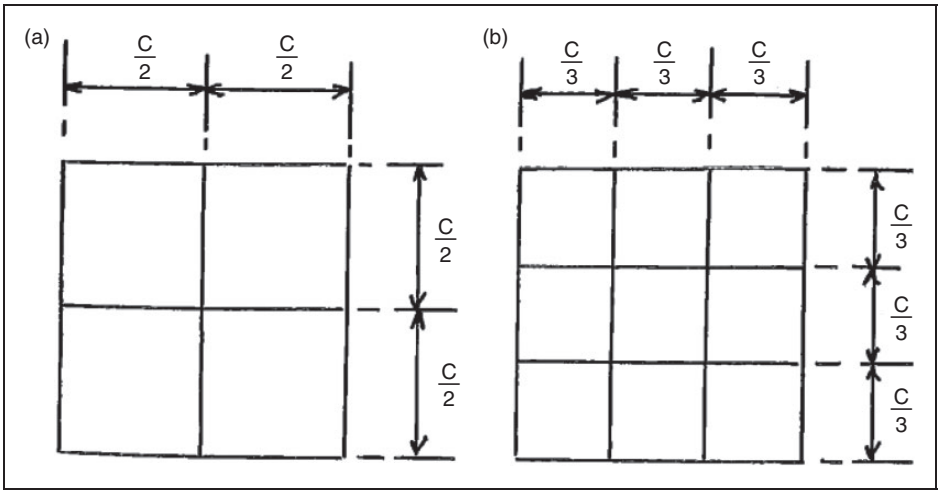

Figure 6. Cross-sections of (a) 2×2 and (b) 3×3 multicellular square tubes.

1060 square tubes with C/H = 53.3 ($\phi = 0.075$) and loaded statically. One of the tubes was divided internally into four equal square cells (i.e. 2×2 section in Figure 6(a)). It turns out that the energy absorbing factor is 1.98 times greater than the corresponding value for the single-cell square tube, which again demonstrates the superiority of multicellular sections. The corresponding ratio is 1.47 in Figure 7 for aluminium alloy 6060T4 sections.

Several authors have used theoretical and/or numerical methods to study the behaviour of multicellular sections. For example Kim[21] used a numerical scheme to study the dynamic crushing behaviour of square aluminium alloy 6063T7 multicellular tubes having a square or circular cells at each corner of the square cross-section. It is estimated that ψ is 0.89, 2.36 and 2.57 for a square tube and for multicellular square tubes with circular tubes or square tubes at the corners, respectively. This revealed a significant advantage of adding internal members in square tubes.

Some static experimental tests are reported by Zhang and Zhang[35] on a square multicellular section and a hexagonal multicellular section made from aluminium alloy 6061O. It is evident that the behaviour was stable and $\psi = 1.39$ with $\phi = 0.19$ and $\psi = 1.28$ with $\phi = 0.10$ for the square and hexagonal multicellular sections, respectively. Zhang and Zhang[36] have continued their theoretical studies by exploring the static behaviour of components of cellular structures, for example various intersections of internal plates.

Wu et al.[19] have studied the impact response of a square section divided into four cells (2×2 in Figure 6(a)) and two tubes with five cells having a square box at each corner. The axial crushing of a regular square section gave $\psi = 1.84$ when taking $\varepsilon_r = 0.12$ for aluminium alloy 6063T5. This value of ψ was corrected to allow complete crushing with an effective crushing distance of $0.75 \times$ the initial tube length. Similarly, $\psi = 2.99$ and $\psi = 3.45$ (average of two tests) for the square tubes with four and five cells, respectively. It is possible that the effective crushing distance is different for the three cases, but no information was offered in the paper on this point.

Figure 8 contains the experimental data reported in literature[19,29,32,34,35] on aluminium alloy square tubes and square tubes with four cells (+and × arrangements of the internal members) and the theoretical predictions of Zhang et al.[31] for aluminium alloy 6060T4 multi cells having the same geometries. Despite the range of aluminium alloys (AA6061O, 1060, 6060T4, 6163T5) in Figure 8, there is a similar trend of the results with ϕ. It is evident that the multicellular sections have larger values of ψ for a similar value of ϕ.

An experimental test was reported by Fang et al.[37] on a 3×3 multicellular square tube subjected to a static axial crushing force. The tube is made from aluminium alloy 6063-O and the results show that

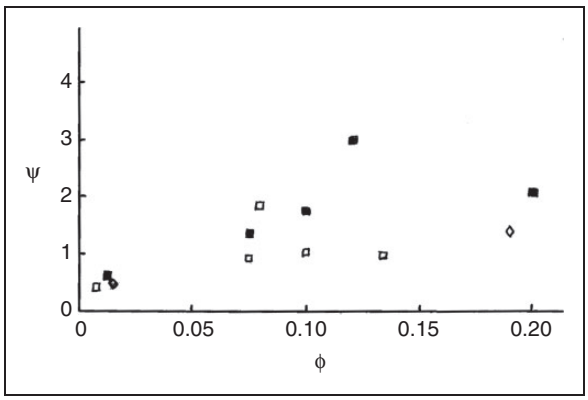

Figure 8. Energy-absorbing effectiveness factor versus solidity ratio for aluminium alloy multicellular square tubes.[19,29,31,32,34,35] □: square tube, ■: 2×2 section, ◇: square tube with internal members across diagonals.

$\psi = 1.77$ and $\phi = 0.16$. This value of ψ is higher than that in Figure 7 ($\psi = 1.66$, $\phi = 0.075$), but it is expected to be somewhat higher according to the increase in ψ with ϕ in Figures 4 and 8 for multicellular sections.

Zhang and Zhang[38] have explored the static axial crushing of circular columns with several internal structural arrangements to give multiple cells and made from aluminium alloy 6061O. The values of ψ are 1.58, 2.20 and 2.30 for double, triple and quadruple cells, respectively, which are to be compared with $\psi = 1.87$ ($\phi = 0.13$) for a single column (i.e. circular tube with no internal divisions). Thus, the double section circular tube ($\phi = 0.18$) is less effective than a hollow tube so that the additional material is a less efficient way to absorb the axial crushing energy. The most effective multiple cell case (quadruple cell with $\phi = 0.22$) is only 23% better than a hollow tube. This situation occurs because the axial energy absorbing capacity of a hollow circular tube is particularly efficient. It should also be noted that with an increase in internal structure the dimensionless effective crushing distance decreases from 0.68 to 0.64 which affects the total energy absorbed by a multiple cell section.

Alavi Nia and Khodabakhsh[39] have explored the effect of the radial distance between concentric thin-walled tubes made of aluminium alloy sheet 1050 and subjected to static and low-velocity mass impact axial crushing loads. The values of ψ for the static experimental tests on concentric tubes are 4.81–5.14 ($\phi = 0.05$–0.06) for the three specimens listed in table 11 of Alavi Nia and Khodabakhsh.[39] These values are to be contrasted with $\psi = 4.18$ for a single circular tube ($\phi = 0.04$). The values of ψ for the two experimental values given in table 10 of Alavi Nia and Khodabakhsh[39] for the mass impact loadings at 8 m/s of concentric tubes are 10.10 ($\phi = 0.06$) and 12.04 ($\phi = 0.09$), which are significantly larger than the quasi-static values estimated above. A finite element analysis is used to examine the problem, and some

comments are offered on the effect of radial distances between the two concentric tubes.

Jusuf et al.[15] have studied the axial mass impact behaviour of several arrangements of two concentric square tubes.[40] One arrangement (DW) had no connections between the inner and outer walls, whereas tubes CR were connected by webs at the four corners and tubes designated MR were joined at the middle of the four sides. The square tubes were made from mild steel St37 and were struck axially with a mass travelling up to an initial velocity of 7.08 m/s. For comparison purposes, the regular square tube has a value $\psi = 0.67$ and $\phi = 0.091$ when using an engineering rupture strain of 0.36[40] and using the experimental value for the absorbed energy multiplied by the ratio of the effective crushing distance of 0.75 mm × 180 mm and the actual crushing distance of 106.1 mm. Similarly, the double square tubes DW, CR and MR have $\psi = 0.93$, 1.95 and 1.86, respectively. The corresponding solidity ratios are 0.136, 0.162 and 0.176, respectively. It is evident that using concentric tubes is advantageous for efficient energy absorbing purposes, particularly when the tubes have connecting webs.

Tang et al.[33] have used a numerical finite element method to explore the effectiveness of internal web arrangements to create multiple cells in circular and square tubes. The behaviour is explored for three particular tubes made from aluminium alloy 6060T4 and an axial impact velocity of 10 m/s. It turns out that ψ is 1.02, 1.78 and 2.59 for a regular square tube ($\phi = 0.1$), quadruple square tube (2×2 section in Figure 6(a) with $\phi = 0.1$) and a circular tube having a central circular tube attached with four radial webs to the outer tube ($\phi = 0.13$). Clearly, a square tube with four cells is more effective than a regular square tube and the multicellular circular case is significantly more effective than both. Due to the higher efficiency of circular tubes, the authors have also used the numerical analysis to explore the effect of various factors on the behaviour of cylindrical multiple cell columns.

Polygonal sections

Alavi Nia and Hamedani[20] have reported some experimental results on thin-walled tubes with several different cross-sections. The tubes have the same axial length, average cross-sectional areas and are made from aluminium alloy 3003H12 material and are subjected to static axial crushing forces. Equation (3) is used to estimate ψ when taking the uniaxial rupture strain as 0.25. Figure 9 provides a summary of these calculations from which it is clear that a circular tube has the highest value of ψ for both wall thicknesses of 1 and 1.5 mm. The triangular shape for H = 1.5 mm has the smallest value for all seven sections having H = 1.5 mm. Only four different sections were tested for the 1 mm thick sheet, and the pyramidal case came out with the smallest value of ψ. The trends in this figure are similar to those in figure 5 of Jones[1] for mild steel sections. The associated solidity ratios are given in the abscissa and range between 0.10 and 0.17 for the plate thicknesses of 1.5 mm.

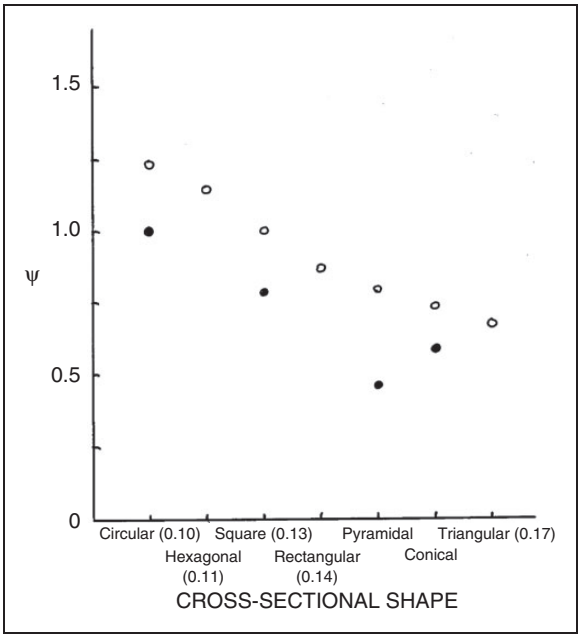

Figure 9. Variation of energy-absorbing effectiveness factor with the cross-sectional shape of an aluminium alloy 3003H12 tube crushed axially.[20] ●: H = 1.0 mm, ○: H = 1.5 mm (ϕ for H = 1.5 mm thick tubes is given in parentheses).

Zhang and Zhang[14] have reported on the static axial compressive behaviour of square (C/H = 33.3, $\phi = 0.12$), hexagonal, octagonal and two rhombic sections. All of the sections were made from 1.2 mm thick Q235 steel having an average flow stress of 270.9 MPa. Calculations reveal that the energy-absorbing effectiveness factors are within the narrow range of $\psi = 0.49$–0.50 for all five sections. In other words, the parameter ψ in this case does not discriminate between the different cross-sectional shapes. It is interesting that the results are very similar to the values of ψ obtained by Costas et al.[41] for irregular steel box sections. It should be noted that the mean crushing load of the octagonal section ($\phi = 0.05$) is twice that found for the square tube which has one-half of the cross-sectional area.

Alavi Nia and Parsapour[32] have constructed thin-walled tubes having a dozen different cross-sections, two-thirds of which have internal webs creating three or four cells. Aluminium sheets with thickness of 0.1 mm were used to manufacture the test specimens which were subjected to quasi-static crushing forces. It turns out that ψ is approximately equal to 0.58, 0.56, 0.44 and 0.33 for the octagonal ($\phi = 0.0075$), hexagonal ($\phi = 0.0077$), square ($\phi = 0.008$) and triangular ($\phi = 0.011$) cross-sections, respectively. This is the same trend as those shown in figure 5 of Jones[1] and Figure 9 in this paper. The incorporation

of three or four cells leads to increases in ψ for the four geometries with the highest value of $\psi = 0.67$ ($\phi = 0.011$) for the three-cell hexagonal and the four-cell octagonal cases, both with the cell walls attached to the centres of the sides, rather than at the corners. In fact, it was observed that in every case, the cell walls emanating from the tube corners led to smaller values of ψ when compared to those originating from the centre of a tube side. This behaviour occurs probably because the cell walls strengthen the resistance to wrinkling of the tube sides, which are weaker when compared with the corners.

The energy-absorbing effectiveness factor, ψ, was obtained by Fan et al.[42] for tubular sections having hexagonal, octagonal and 12- and 16-sided star polygonal shapes. The sections were made from a low carbon steel (ASTM A36) and subjected to quasi-static axial crushing. The authors obtained ψ values of 0.54, 0.68, 0.80 and 0.55 for the hexagonal, octagonal, 12- and 16-sided star shapes, respectively. All cross-sections had a solidity ratio $\phi = 0.094$, approximately. Thus, the best tubular shape in this study for absorbing crushing energy is the 12-sided star since it uses the material most effectively. However, some fracture was observed in the 12- and 16-sided star polygonal sections.

Xiang et al.[7] have collected numerical and experimental data from previously published work to examine a number of key performance indicators for the static behaviour of polygonal and multicellular tubes, but the authors did not consider the energy-absorbing effectiveness factor (ψ) defined by equation (1). However, in order to compare the data from the various studies, the authors have used the solidity ratio, or relative density, ϕ, which was introduced originally by Pugsley (see Jones[8]) and is defined by equation (7). The material properties were not presented in the paper, so it is assumed that $\rho = 7850\,\mathrm{kg/m^3}$, $\sigma_o = 250\,\mathrm{MPa}$ and $\varepsilon_r = 0.33$ for the mild steel polygonal tubes. It follows that ψ can be obtained from the data in figure 5 of Xiang et al.[7] when using equation (3). The data in Figure 5 is quite scattered, but generally speaking, it is evident that ψ follows the same trend as in Figure 9 in the sense that ψ increases in the sequence triangular, square, hexagonal, octagonal with the circular tubes having the highest value of ψ. The values of ψ for each type of tube increase with increase of the solidity ratio, ϕ, as noted previously. The authors have also discussed the aluminium alloy 6060T4 multicellular tubes studied numerically in Zhang et al.[31] and discussed in '*Multicellular sections*' section.

Discussion

It is evident from the previous discussion that a wide range of cross-sections for tubular members has been studied experimentally, numerically and theoretically in order to seek the most efficient shape to absorb energy for crashworthiness applications in passenger transport, for example. The energy-absorbing effectiveness factor, ψ, introduced by equation (1), has been used to rank the effectiveness of a given energy absorbing system. It can be used to study the effectiveness of a system made from different ductile materials or to compare the effectiveness of different designs made from a given material or of different materials.

The comparisons in this paper are made using the solidity ratio which is defined by equation (7). It is evident from Figure 1 that ψ increases with an increase in ϕ for square and circular tubes crushed axially, both under static and impact loadings. A similar behaviour is shown in Figure 3 for triangular tubes. However, it is particularly striking in Figures 4, 7 and 8 that ψ increases significantly for multicellular sections. Figure 7 reveals that a 5×5 multicellular section has a value for ψ which is double the value for a corresponding square tube having the same value of ϕ. The results appear to indicate that a saturation condition is being approached with an increase in the complexity of a cross-section. They show the importance of the disposition of the internal structure, as is also observed in Zhang et al.[31] where the value of ψ was dependent on the arrangement of the internal structure for the same amount of material. It is interesting to note that in Zhang and Zhang[38] a circular tube having two cells is less effective than a regular hollow circular tube despite having a larger value of ϕ, though the addition of further cells does turn out to be more effective. Thus, the addition of more material is not always more effective.

Figure 4 also reveals the important enhancement of the energy absorbing capacity by infilling tubes with foam, for example or in Figure 2 with an internal pressure. It is observed that the foam in Figure 4 is less effective for the thicker tube specimens which is due possibly to the interaction effect between the foam and the tube wall being less significant for the thicker tubes. Actually, a somewhat similar phenomenon might occur in Figure 2 where the enhancement of ψ caused by an internal pressure is least for the thickest circular tubes that have a smaller circumferential stress due to the internal pressure.

Impact loadings can also further increase the value of ψ as revealed in Figure 1.

It is important to recognise that an increase in ψ could cause an increase in the mean crushing load, as indicated by equation (2). This situation would lead to larger decelerations. Potentially, these increased decelerations could pose difficulties in structural design and in satisfying the human impact injury criterion. Also large values of ψ could lead to fracture of the material, although it is possible to cater for this phenomenon in the denominator of equations (1) and (2).

The results in Figure 9 for single sections reveal the importance of the cross-sectional geometry on the value of ψ with a circular tube having the largest

value and a triangular section the smallest, despite having a larger value of ϕ.

It should be noted that when a structural system is made from a single material, then the energy-absorbing effectiveness factor given by equation (3) can be written in the form

$$\psi = \frac{\rho}{\sigma_o \varepsilon_r} \times SEA \tag{10}$$

where SEA is the dimensional specific energy absorbed or the energy absorbing capacity per unit mass. ψ is dimensionless and provides a measure of how effective or efficient the system is in absorbing energy. It could be regarded as an environmental factor, since it suggests the selection of a design which requires the least amount of material and the most effective disposition of that material.

It is noted in some cases that the energy-absorbing effectiveness factor, ψ, is larger than 1.0. This situation arises because the actual potential energy that could be absorbed by the material in the denominator of equation (1) ignores several features. For example the influence of strain rate sensitive material properties for impact loadings is not considered, although it could be retained in the denominator of the equation, but it is ignored in this paper in order to retain a simple expression. In the case of foam filled tubes, a favourable interaction develops between a foam filling and the tube walls leading to an enhanced energy absorption. Triaxiality effects could also influence the energy absorbed in a crushed tube. Also some of the dominant axial stresses in a tube are compressive (σ_x), whereas the materials tests reported in most studies have been obtained from a standard uniaxial tensile test. In fact, for a simple biaxial case with $\sigma_x = -\sigma_y$, then the equivalent stress $\sigma_e = (3)^{1/2}\sigma_x$ and the equivalent strain rate $\dot{\varepsilon_e} = 2\dot{\varepsilon}_x/\sqrt{3}$. Thus, taking a simple view (i.e. ignoring σ_z), the work rate $\sigma_e \dot{\varepsilon}_e = 2\sigma_x \dot{\varepsilon}_x$ is twice the energy absorbed in a standard uniaxial tensile test.

The denominator of the energy-absorbing effectiveness factor, which is defined by equation (1), is the energy absorbed in a standard uniaxial tensile test conducted on the material(s) up to rupture. This simple expression provides a basis which is the same for all calculations of ψ regardless of the structural designs and material(s). Nevertheless, it would be possible to cater for the more complex behaviour of the materials in the denominator of equation (1) if the information was available.

In order to calculate ψ, the energy absorbed in the numerator of equation (1) should be the maximum value which occurs when the effective crushing displacement, or the bottoming-out displacement, is reached. Unfortunately, a paucity of information is usually given on this point in many papers so that it becomes necessary to use the dimensionless value 0.75 for δ_e/L. However, it is quite possible for some multicellular cross-sections that the effective crushing distance is smaller because of the more complex crushing deformations which might hinder the regular behaviour to the bottoming-out condition. In this case, the associated value of ψ would be smaller.

An illustration of a practical application of the energy-absorbing effectiveness factor is that the machining of grooves in steel cylindrical shells[24] is not an efficient design since the associated values of ψ are smaller when compared with a cylindrical shell without grooves.

Costas et al.[41] have studied the static and dynamic axial crushing behaviour of car frontal impact energy absorbers. These 1 mm thick irregularly shaped boxes are made from cold formed steel sheets and several different core materials are investigated. In the case without any core material, the experimental data can be used to calculate the energy-absorbing effectiveness factors $\psi = 0.47$ and $\psi = 0.50$ for the static and impact loadings, respectively. The corresponding values of ψ for the same boxes with a GFRP core structure are slightly smaller, or $\psi = 0.45$ and $\psi = 0.47$ when the contribution to the potential energy absorption by the core is not considered in the denominator of ψ. Thus, the true values of ψ would be even smaller when accounting for this extra energy in the denominator. The experimental results indicate that the infilling of this particular energy absorber is not advantageous from the perspective of the energy-absorbing effectiveness factor. The ratio can be taken as $C/H = 100$ ($\phi = 0.04$), approximately, for the particular geometry in Costas et al.[41]

Kohar et al.[43] have developed a front rail designed to absorb axial crushing energies during a vehicle collision. The authors have crushed axially the aluminium alloy 6063T6 rails at an initial impact velocity of 8 m/s in a sled test arrangement. This experimental set-up imparts a maximum axial crush displacement of 125 mm, while the rails have an initial length of 464 mm. If it is assumed that the dimensionless effective crushing distance (δ_e/L) for both rail geometries in Kohar et al.[43] is 0.75, then the energies absorbed in the experiments should be multiplied by $0.75 \times 464/125 = 2.784$ when estimating the energy-absorbing effectiveness factor. Thus, equation (6) gives $\psi' = 3.21$ with $\phi \approx 0.105$ for the case shown in figure 1 of Kohar et al.[43] which has a somewhat similar design to the triple cell system in Figure 5(b), except that it is closer to a rectangular shaped cross-section with a 7° angle between the long sides. The other more complex cross-sectional shape in figure 2 of Kohar et al.[43] with $\phi \approx 0.12$ has $\psi' = 4.48$. If, instead of using the energies absorbed by the rails for these calculations, the mean crushing force is substituted into equation (5), then it turns out that slightly higher values are obtained, namely $\psi = 3.38$ and $\psi = 4.67$ for the cases in figures 1 and 2 of Kohar et al.,[43] respectively. It is noted that in Hsu and Jones[3] that $\psi = 4.14$ and $\psi' = 5.72$ for circular tubes made

from the same material (aluminium alloy 6063T6) and crushed axially.

Conclusions

The dimensionless energy-absorbing effectiveness factor has the merit that it reveals the most efficient or effective structural system, or energy-absorbing device, and suggests which system from many competing designs uses the material from which it is made in the most effective way. Thus, it is also a type of environmental factor since it explores the energy potential of the entire system, and the largest value of ψ is associated with the least amount of material used in the construction. The energy-absorbing effectiveness factor has been discussed in this paper and is used to study the behaviour of tubes with a rich variety of cross-sectional shapes subjected to axial static and impact loadings. Generally speaking, it is observed that the tubes with multicellular cross-sections offer improved energy absorbing capacity compared with single cell tubes. The experimental and numerical results have been expressed in terms of the solidity ratio, or relative density, which is a useful parameter for ordering and interpreting the results.

The energy-absorbing effectiveness factor is another dimensionless factor in the armoury for designers and is complementary to the well-known existing design parameters. It can be used for any type of material, or combinations of materials, and any structural geometry subjected to static or dynamic loadings.

Declaration of Conflicting Interests

The author(s) declared no potential conflicts of interest with respect to the research, authorship, and/or publication of this article.

Funding

The author(s) received no financial support for the research, authorship, and/or publication of this article.

References

1. Jones N. Energy-absorbing effectiveness factor. *Int J Impact Eng* 2010; 37: 754–765.
2. Boria S, Obradovic J and Belingardi G. Experimental and numerical investigations of the impact behaviour of composite frontal crash structures. *Compos Part B Eng* 2015; 79: 20–27.
3. Hsu SS and Jones N. Quasi-static and dynamic axial crushing of thin-walled circular stainless steel, mild steel and aluminium alloy tubes. *Int J Crashworthiness* 2004; 9: 195–217.
4. Jones N. Energy-absorption effectiveness of thin-walled structures under static and dynamic axial crushing loads. In: Alves M and Jones N (eds) Impact loading of lightweight structures.WIT Press, Southampton UK and Boston US. *WIT Trans Eng Sci* 2005; 49: 273–287.
5. Chen W and Wierzbicki T. Relative merits of single-cell, multi-cell and foam-filled thin-walled structures in energy absorption. *Thin-Walled Struct* 2001; 39: 287–306.
6. Belingardi G, Beyene AT and Jichuan D. Energy absorbing capability of GMT, GMTex and GMT-UD composite panels for static and dynamic loading-experimental and numerical study. *Compos Struct* 2016; 143: 371–387.
7. Xiang Y, Yu TX and Yang L. Comparative analysis of energy absorption capacity of polygonal tubes, multi-cell tubes and honeycombs by utilising key performance indicators. *Mater Design* 2016; 89: 689–696.
8. Jones N. *Structural impact*. 2nd ed. Cambridge, UK: Cambridge University Press, 2012.
9. Lu G and Yu TX. *Energy absorption of structures and materials*. Cambridge, UK: Woodhead Publishing Limited, 2003.
10. Abramowicz W and Jones N. Dynamic progressive buckling of circular and square tubes. *Int J Impact Eng* 1986; 4: 243–270.
11. Abramowicz W and Jones N. Dynamic axial crushing of square tubes. *Int J Impact Eng* 1984; 2: 179–208.
12. Schneider FD and Jones N. Impact of Thin-Walled High-Strength Steel Structural Sections. *Proc IMechE, Part D: J Automobile Engineering* 2004; 218: 131–158.
13. DiPaolo BP and Tom JG. A study on an axial crush configuration response of thin-wall, steel box components; the quasi-static experiments. *International Journal of Solids and Structures* 2006; 43: 7752–7775.
14. Zhang X and Zhang H. Experimental and numerical investigation on crush resistance of polygonal columns and angle elements. *Thin-Walled Struct* 2012; 57: 25–36.
15. Jusuf A, Dirgantara T, Gunawan L, et al. Crashworthiness analysis of multi-cell prismatic structures. *Int J Impact Eng* 2015; 78: 34–50.
16. Zhang X, Wen Z and Zhang H. Axial crushing and optimal design of square tubes with graded thickness. *Thin-Walled Struct* 2014; 84: 263–274.
17. Zhang X and Zhang H. Crush resistance of square tubes with various thickness configurations. *Int J Mech Sci* 2016; 107: 58–68.
18. Yamashita M, Gotoh M and Sawairi Y. Axial crush of hollow cylindrical structures with various polygonal cross-sections; numerical simulation and experiment. *J Mater Process Technol* 2003; 140: 59–64.
19. Wu S, Zheng G, Sun G, et al. On design of multi-cell thin-wall structures for crashworthiness. *Int J Impact Eng* 2016; 88: 102–117.
20. Alavi Nia A and Hamedani JH. Comparative analysis of energy absorption and deformations of thin walled tubes with various section geometries. *Thin-Walled Struct* 2010; 48: 946–954.
21. Kim H-S. New extruded multi-cell aluminium profile for maximum crash energy absorption and weight efficiency. *Thin-Walled Struct* 2002; 40: 311–327.
22. Langseth M and Hopperstad OS. Static and dynamic axial crushing of square thin-walled aluminium extrusions. *Int J Impact Eng* 1996; 18: 949–968.
23. Jensen O, Langseth M and Hopperstad OS. Experimental investigations on the behaviour of short to long square aluminium tubes subjected to axial loading. *Int J Impact Eng* 2004; 30: 973–1003.

24. Salehghaffari S, Tajdari M, Panahi M, et al. Attempts to improve energy absorption characteristics of circular metal tubes subjected to axial loading. *Thin-Walled Struct* 2010; 48: 379–390.
25. Zhang XW and Yu TX. Energy absorption of pressurised thin-walled circular tubes under axial crushing. *Int J Mech Sci* 2009; 51: 335–349.
26. Hu LL, Zeng ZH and Yu TX. Axial crushing of pressurized cylindrical tubes. *Int J Mech Sci* 2016; 107: 126–135.
27. Hong W, Jin F, Zhou J, et al. Quasi-static axial compression of triangular steel tubes. *Thin-Walled Struct* 2013; 62: 10–17.
28. Fan Z, Lu G, Yu TX, et al. Axial crushing of triangular tubes. *Int J Appl Mech* 2013; 5: 1350008–1–1350008-21.
29. Zhang X and Zhang H. Energy absorption of multi-cell stub columns under axial compression. *Thin-Walled Struct* 2013; 68: 156–163.
30. Santosa SP, Wierzbicki T, Hanssen AG, et al. Experimental and numerical studies of foam-filled sections. *Int J Impact Eng* 2000; 24: 509–534.
31. Zhang X, Cheng G and Zhang H. Theoretical prediction and numerical simulation of multi-cell square thin-walled structures. *Thin-Walled Struct* 2006; 44: 1185–1191.
32. Alavi Nia A and Parsapour M. Comparative analysis of energy absorption capacity of simple and multi-cell thin-walled tubes with triangular, square, hexagonal and octagonal sections. *Thin-Walled Struct* 2014; 74: 155–165.
33. Tang Z, Liu S and Zhang Z. Analysis of energy absorption characteristics of cylindrical multi-cell columns. *Thin-Walled Struct* 2013; 62: 75–84.
34. Alavi Nia A and Parsapour M. An investigation on the energy absorption characteristics of multi-cell square tubes. *Thin-Walled Struct* 2013; 68: 26–34.
35. Zhang X and Zhang H. Energy absorption limit of plates in thin-walled structures under compression. *Int J Impact Eng* 2013; 57: 81–98.
36. Zhang X and Zhang H. Numerical and theoretical studies on energy absorption of three-panel angle elements. *Int J Impact Eng* 2012; 46: 23–40.
37. Fang J, Gao Y, Sun G, et al. On design of multi-cell tubes under axial and oblique impact loads. *Thin-Walled Struct* 2015; 95: 115–126.
38. Zhang X and Zhang H. Axial crushing of circular multi-cell columns. *Int J Impact Eng* 2014; 65: 110–125.
39. Alavi Nia A and Khodabakhsh H. The effect of radial distance of concentric thin-walled tubes on their energy absorption capability under axial dynamic and quasi-static loading. *Thin-Walled Struct* 2015; 93: 188–197.
40. Gunawan L, Sitompul SA, Dirgantara T, et al. Material characterisation and axial crushing tests of single and double-walled columns at intermediate strain rates. *J Mech Eng* 2014; 10: 19–36.
41. Costas M, Diaz J, Romera LE, et al. Static and dynamic axial crushing analysis of car frontal impact hybrid absorbers. *Int J Impact Eng* 2013; 62: 166–181.
42. Fan Z, Lu G and Liu K. Quasi-static axial compression of thin-walled tubes with different cross-sectional shapes. *Eng Struct* 2013; 55: 80–89.
43. Kohar CP, Zhumagulov A, Brahme A, et al. Development of high crush efficient, extrudable aluminium front rails for vehicle lightweighting. *Int J Impact Eng* 2016; 95: 17–34.

Appendix

Notation

A	cross-sectional area
A_e	enclosed area
C	side length of a square tube
g	gravitational constant
G	impact mass
H	thickness
P	axial force
P_m	mean value of axial force
R	radius
V	volume of material
V_o	impact velocity
δ	axial displacement
δ_e	effective crushing displacement
δ_f	final value of axial displacement
ε_x	axial strain
ε_e	equivalent strain
ε_r	rupture strain
$\dot{\varepsilon}$	strain rate
ρ	density
σ_x	axial stress
σ_e	equivalent stress
σ_o	mean flow stress
σ'_o	dynamic flow stress
σ_y, σ_u	yield and ultimate stresses
ϕ	solidity ratio, equation (7)
ψ	energy-absorbing effectiveness factor, equation (1)
ψ'	dynamic energy-absorbing effectiveness factor